

Synthesis of $\text{SO}_4^{2-}/\text{ZrO}_2$ Solid Acid and $\text{Na}_2\text{O}/\text{ZrO}_2$ Solid Base Catalysts Using Hydrothermal Method for Biodiesel Production from Low-Grade Crude Palm Oil

Sri Setyaningsih¹, Maisari Utami², Akhmad Syoufian³, Eddy Heraldy⁴,
Nasih Widya Yuwono⁵, and Karna Wijaya^{3*}

¹Department of Science Education, Faculty of Teacher Training and Education, Universitas Islam Lamongan, Jl. Veteran No. 53A, Lamongan 62211, Indonesia

²Department of Chemistry, Faculty of Mathematics and Natural Sciences, Universitas Islam Indonesia, Jl. Kaliurang km. 14, Yogyakarta 55584, Indonesia

³Department of Chemistry, Faculty Mathematics and Natural Science, Universitas Gadjah Mada, Sekip Utara, PO BOX BLS 21, Yogyakarta 55281, Indonesia

⁴Department of Chemistry, Faculty of Mathematics and Natural Sciences, Sebelas Maret University, Jl. Ir. Sutami 36A, Surakarta 57126, Central Java, Indonesia

⁵Department of Soil Science, Faculty of Agriculture, Universitas Gadjah Mada, Jl. Flora, Bulaksumur, Yogyakarta 55281, Indonesia

* **Corresponding author:**

email: karnawijaya@ugm.ac.id

Received: April 20, 2021

Accepted: October 18, 2021

DOI: 10.22146/ijc.65404

Abstract: Biodiesel is a renewable energy source that can be produced through esterification as well as transesterification reactions. This work presents a series of zirconia catalysts synthesized by hydrothermal method on various concentrations in acidic (H_2SO_4 0.3, 0.5, and 0.7 M) and basic (NaOH 1, 2, 3, and 4 M) solution to get a catalyst with the highest acidity or basicity. Characterizations of the catalysts were performed by FTIR, XRD, SEM-EDX, surface area analysis, acidity, and basicity test. The most active acid catalyst activity was evaluated for the esterification of low-grade crude palm oil (LGCPO), while the solid base catalyst was utilized for the transesterification reaction. The solid acid catalyst of 0.7 M $\text{SO}_4^{2-}/\text{ZrO}_2$ 60 °C; 24 h was denoted as the most active acid catalyst with a total acidity of 1.86 mmol g^{-1} , while 4 M $\text{Na}_2\text{O}/\text{ZrO}_2$ 60 °C; 24 h catalyst was considered as the solid base catalyst with the highest total basicity of 3.75 ± 0.12 mmol g^{-1} . The optimized acid catalyst exhibited a 31 times higher acidity than commercial ZrO_2 . The concentration of free fatty acids (FFA) decreased to 68.87% in the esterification reaction. The solid base catalyst of 4 M $\text{Na}_2\text{O}/\text{ZrO}_2$ 60 °C; 24 h successfully converted LGCPO into biodiesel by 68.55% through a transesterification reaction.

Keywords: $\text{SO}_4^{2-}/\text{ZrO}_2$ solid acid catalyst; $\text{Na}_2\text{O}/\text{ZrO}_2$ solid base catalyst; esterification; transesterification; biodiesel

■ INTRODUCTION

More than 90% of the consumption of energy sources in the world is currently based on fossil fuels [1]. Fossil fuels are a limited source of energy. One effort to tackle the scarcity of fossil fuels is creating alternative fuels. Biodiesel is a monoalkyl ester compound that has the potential to be an alternative renewable fuel. Biodiesel has been widely accepted in the market because of its low

sulfur content and higher octane number than petrodiesel [1]. The presence of 11–15% oxygen in biodiesel can accelerate the combustion process and reduce the number of particulates, soot, and CO gas. Therefore, greenhouse gas emissions are low [2-3].

Biodiesel is formed from the conversion of free fatty acids and triglycerides to methyl esters. The source of triglycerides (TG) and free fatty acids (FFA) are

generally contained in vegetable and animal oils [4]. Low Grade Crude Palm Oil (LGCPPO) produced by the oil industry as a waste containing triglycerides and FFA can be used as raw material for forming methyl esters [5]. LGCPPO has been used as raw material for low grade soap and boiler fuel. Therefore, processing LGCPPO into biodiesel can increase its value. LGCPPO raw materials are high abundance and inexpensive, so they have the potential to be developed on a large scale with low production costs [6].

In general, biodiesel is produced through a transesterification reaction by adding a base catalyst when the FFA number in the raw material is < 2 wt.%. Highly FFA will affect the formation of biodiesel. The concentration of FFA exceeds more than 1%, causing saponification when catalyzed using base catalysts such as NaOH [7]. The soap formation will complicate the separation process and cause a low yield. A two-step process through esterification reaction using an acid catalyst followed by transesterification using a base catalyst is employed to overcome this problem [8]. The acid catalyst is needed to reduce the concentration of FFA in the raw material by the esterification reaction [9]. Esterification is a reversible reaction that aims to reduce the concentration of FFA using an acid catalyst, where one mole of FFA will react with one mole of alcohol to form one mole of biodiesel and one mole of water [10-11].

Most methyl ester formation reactions are catalyzed by homogeneous base catalysts such as NaOH and KOH [1,8]. However, the application of homogeneous catalysts causes the separation process to be complicated, reactor corrosion, and an increasing amount of pollutants [12]. On the other hand, heterogeneous catalysts have advantages such as being easily separated and having low pollutants [8,13]. Therefore, the method of heterogeneous catalyst synthesis that is safe for the environment with low production costs is being developed [4]. The ideal characteristic of heterogeneous catalysts is a strong acid or base site, hydrophobic surface area, large pores interconnected, high activity, selective, stable to pressure and temperature [14-15]. For example, zirconia dioxide (ZrO_2) can be used as a catalyst and supporting material because it has redox activity and bifunctionality for both

acidity and basicity properties [16-17]. Research using heterogeneous acid and base catalysts from ZrO_2 to produce biodiesel has evolved today [18-19].

Sulfated zirconia as a catalyst has been successfully synthesized using the sol-gel method, precipitation, and wet impregnation. The weakness of the sol-gel method is the difficulties of the preparation process on pH control, composition, and temperature that affect the synthesized material. In addition, the precursors are expensive. The route of material synthesis using the precipitation method is easier, but the shape of the particles is irregular, and the size distribution is wide. The material synthesized using the hydrothermal method has a lower crystallization temperature and agglomeration rate. The resulted powder is good without calcination. The shape and distribution of particle size are controlled [20]. However, no previous publication has developed a hydrothermal method to investigate the activity of monoclinic zirconia as an acid and base catalyst.

Sulfated zirconia (SO_4^{2-}/ZrO_2) has been reported to have super acidic properties [21]. The strong acid character is caused by the presence of sulfate ions which bind to the substrate [22]. Its high acid strength and combination of acid sites (Brønsted and Lewis) are the most significant factors in enhancing selectivity and activity [11]. The superiority of this catalyst is its high activity at relatively low temperatures [23]. SO_4^{2-}/ZrO_2 has a catalytic activity that can convert hydrocarbons at low temperatures [24]. The lack of SO_4^{2-}/ZrO_2 catalysts are the limited surface area that affects the acidity, so some modifications are developed to increase the acidity of the catalyst. The physical and chemical properties of this catalyst are determined by the sulfation method [25]. Synthesis in hydrothermal conditions offers significant advantages, such as easily controlling particle size and morphology by optimizing synthesis parameters and conditions [26]. Catalytic activities of SO_4^{2-}/ZrO_2 can be improved by optimizing the preparation conditions to enhance the zirconia framework's acidic strength [27].

The catalytic activity of ZrO_2 in the transesterification reaction is not great because of its

weak basic properties. On the other hand, the existence of empty sites on the surface of ZrO_2 facilitates molecular dispersion to be used as an excellent supporting material [28]. The prospect of supporting basic species on metal oxide supports is expected to tune the basicity and redox properties, leading to a more active and selective catalytic system [29]. The common method used to increase the basic strength of the catalyst is by modifying a supporting material using alkali and alkaline earth metals [30]. It is well-known that alkali metals (such as Li, Na, and K) or alkaline earth have good interactions for transesterification reactions and can be applied to supporting materials such as bentonite, Al_2O_3 , SiO_2 , and activated carbon. The metals loading on a supporting material produces heterogeneous catalysts that can increase the transesterification reaction's activity [31]. Modifying the ZrO_2 matrix with NaOH to synthesize heterogeneous base catalysts with high catalytic activity becomes challenging to develop.

Catalyst synthesis using the hydrothermal method is expected to increase the dispersion of SO_4^{2-} or Na^+ in the ZrO_2 matrix and strengthen the acidity or basicity of the catalyst. This research led to synthesizing SO_4^{2-}/ZrO_2 solid acid and Na_2O/ZrO_2 solid base catalyst by hydrothermal method for converting LGCPO to biodiesel. The method is highlighted to enhance the catalytic performance of both catalysts by providing more acid and base sites for the potential applications of biodiesel production. The solid catalysts and the catalytic activities of the obtained product are optimized to obtain the best results.

■ EXPERIMENTAL SECTION

Materials

Commercial zirconium dioxide (ZrO_2) was acquired from Jiaozou Huasu Chemical Co., Ltd (Henan, China). LGCPO was obtained from one of the palm oil factories in Kabupaten Lampung Selatan, Lampung, Indonesia. The analytical reagents were sulfuric acid (H_2SO_4 98%), sodium hydroxide (NaOH), ammonium hydroxide (NH_4OH 25%), methanol (CH_3OH), hydrochloric acid (HCl), potassium hydroxide (KOH), sodium sulfate anhydrous (Na_2SO_4), oxalic acid ($C_2H_2O_4$) and phenolphthalein indicators purchased from Merck.

Instrumentation

The catalysts were characterized using Fourier Transform Infrared Spectrophotometer (FTIR, Shimadzu Prestige-21), Scanning Electron Microscope (SEM, JEOL JSM-6510) combined with Energy Dispersive X-Ray (EDS, JED-2300 Analysis Station) and Surface Area Analyzer (SAA, Quadrasorb EVO Model QDS-30). The transesterification products were analyzed using Gas Chromatography-Mass Spectrometer (GC-MS, Shimadzu QP2010S), Fourier Transform Infrared Spectrophotometer (FTIR, Shimadzu Prestige-21), and Proton Nuclear Magnetic Resonance Spectrometer (1H -NMR, NMR JEOL NMR 500 MHz).

Procedure

Synthesis of SO_4^{2-}/ZrO_2 solid acid and Na_2O/ZrO_2 solid base catalysts

The SO_4^{2-}/ZrO_2 catalysts were synthesized from 5 g of ZrO_2 and 75 mL of H_2SO_4 with various concentrations of 0.3, 0.5, and 0.7 M using the hydrothermal method. After being mixed perfectly, it was put into an autoclave and heated at a temperature of 60 °C for 24 h. The solid mixture and solution were separated by centrifugation at 2500 rpm for 15 min. Finally, the separate solids were heated at a temperature of 105 °C for 24 h [32]. Catalysts that have been synthesized were labeled as 0.3 M SO_4^{2-}/ZrO_2 60 °C; 24 h, 0.5 M SO_4^{2-}/ZrO_2 60 °C; 24 h, and 0.7 M SO_4^{2-}/ZrO_2 60 °C; 24 h. The catalysts were then characterized using FTIR and acidity tests.

The Na_2O/ZrO_2 catalysts were synthesized by a similar method using NaOH 1, 2, 3, and 4 M. The mixture was then heated at a temperature of 60 °C for 12 h in an autoclave. The catalysts were denoted as 1 M Na_2O/ZrO_2 60 °C; 12 h, 2 M Na_2O/ZrO_2 60 °C; 12 h, 3 M Na_2O/ZrO_2 60 °C; 12 h, and 4 M Na_2O/ZrO_2 60 °C; 12 h then characterized using FTIR and basicity test.

Characterization of SO_4^{2-}/ZrO_2 solid acid and Na_2O/ZrO_2 solid base catalysts

Each catalyst was characterized using Fourier Transform Infrared Spectrophotometer (FTIR, Shimadzu Prestige-21). Catalyst powder was diluted to an appropriate concentration of dry KBr with a ratio of 1:10 (catalyst:KBr) and pressed into a pellet using a

compressor. The infrared spectrum was collected at 400–4000 cm^{-1} .

The acidity test of the acid catalyst was carried out using the gravimetric method. First, the empty crucible was weighed as W_0 . Next, a sample of 0.1 g was put into a crucible, heated at a temperature of 105 °C for one hour, then cooled and weighed as W_1 . The crucible containing the sample was placed into a desiccator and then vacuumed. Ammonia was heated then flowed the vapor into a desiccator. The sample was allowed to stand for 24 h and then weighed as W_2 [17]. The acidity test was determined using NH_3 as a basic probe molecule. The total amount of adsorbed ammonia was calculated using the following equation:

$$\text{Total acidity (mmol g}^{-1}\text{)} = \frac{W_2 - W_1}{(W_1 - W_0) \times \text{Mr NH}_3} \times 1000 \quad (1)$$

The catalyst basicity test was carried out using an acid-base titration method. A sample of 0.1 g was mixed with 10 mL of distilled water. The mixture was stirred using a magnetic stirrer for one hour. 3–5 drops of phenolphthalein indicator were added and titrated using 0.01 M HCl. The titration was carried out until it reached the equivalence point and was repeated three times. The total volume of HCl in mL has been obtained was entered into Eq. (2) to obtain the total basicity of the catalyst [33].

$$\text{Total basicity (mmol g}^{-1}\text{)} = \frac{V_{\text{HCl}}(\text{mL}) \times M_{\text{HCl}}(\text{M})}{\text{mass of catalyst (g)}} \quad (2)$$

The $\text{SO}_4^{2-}/\text{ZrO}_2$ catalyst with the highest total acidity and the $\text{Na}_2\text{O}/\text{ZrO}_2$ catalyst with the highest total basicity calcined at various temperatures of 400, 500, 600, 700, and 800 °C, then characterized using X-Ray Diffractometer (XRD, X PHILIPS XPert MPD). The catalyst was ground to a fine powder then placed into a sample holder. Diffractogram was recorded at $2\theta = 10\text{--}45^\circ$ using XRD with an X-ray source of Cu $K\alpha$ radiation ($\lambda = 1.5406 \text{ \AA}$).

The calcined catalyst with the highest total acidity and basicity was characterized using SEM combined with EDX and Surface Area Analyzer (SSA). The analysis of surface topography and composition of the catalyst was carried out with SEM (JEOL JSM-6510) equipped with an EDS (JED-2300 Analysis Station) spectrometer. Carbon tape was attached on the sample stage, and the catalyst

powder was placed on the carbon tape then vacuumed. The energy resolution was 200 eV. The pressure of the SEM chamber was about 10^{-3} Pa. The accelerating voltage was set to 15 kV. The probe current was set to 10 nA. The SEM-EDX analysis was set to 300 sec. The specific surface area and pore size analysis were performed using Quadrasorb EVO Model QDS-30. The catalyst was loaded into analysis stations. The catalyst was degasified to free surfaces from contaminants such as water and oils under a vacuum. The sample was brought to a constant temperature. Then, nitrogen gas flowed to the sample chamber.

The esterification reaction using $\text{SO}_4^{2-}/\text{ZrO}_2$ solid acid catalyst

The raw material of LGCPO was heated at 105 °C to vaporize water and filtered to remove impurities. The molecular weight of LGCPO was determined by saponification, while the concentration of FFA in LGCPO was determined by titration method using a KOH solution [34-35]. The $\text{SO}_4^{2-}/\text{ZrO}_2$ solid acid catalyst has the highest total acidity applied in the esterification reaction.

Optimization of esterification conditions was carried out on three different parameters on wt.% catalyst, the molar ratio of LGCPO to methanol, and reaction time. The $\text{SO}_4^{2-}/\text{ZrO}_2$ solid acid catalyst on 1, 3, 5, and 7 wt.% of the total mass of LGCPO and methanol with the molar ratio of LGCPO: methanol = 1:9 inserted into a three-necked round-bottom flask, followed by methanol at the molar ratio LGCPO: methanol = 1:9. The mixture was magnetically stirred at 600 rpm in an oil bath, maintaining a constant temperature of 45 °C for 10 min. Then 25 g LGCPO was added to the mixture, and the reaction was continued at 55 °C for 20 min. The study of the effect of the molar ratio of LGCPO to methanol on %FFA LGCPO was conducted on ratios of 1:3, 1:6, and 1:12, and reaction times varied for 40 and 60 min. Free Fatty Acid concentrations contained in esterified oil were determined, and the reduction of FFA (%) was calculated using Eq. (3) [36].

$$\text{FFA Reduction (\%)} = \frac{\% \text{FFA LGCPO} - \% \text{FFA esterified oil}}{\% \text{FFA LGCPO}} \times 100\% \quad (3)$$

Transesterification reaction using $\text{Na}_2\text{O}/\text{ZrO}_2$ solid base catalyst

The $\text{Na}_2\text{O}/\text{ZrO}_2$ solid base catalyst with 7 wt.% of the total mass of LGCPO and methanol with the molar ratio of LGCPO: methanol = 1:24 inserted into a three-necked round-bottom flask, followed by methanol at the molar ratio LGCPO: methanol = 1:24. The mixture was magnetically stirred at 600 rpm in an oil bath, maintaining a constant temperature of 45 °C for 10 min. Then, 20 g esterified oil was added to the mixture, and the reaction was continued at 55 °C for 20 min.

The transesterification compound was characterized using FTIR and analyzed using Gas Chromatography-Mass Spectrometer (GC-MS, Shimadzu QP2010S). The formed methyl ester was analyzed using Proton Nuclear Magnetic Resonance Spectrometer ($^1\text{H-NMR}$, NMR JEOL NMR 500 MHz) to identify the %conversion of methyl ester (C_{ME}), which was calculated based on the proton integration of proton between triglycerides (I_{TAG}) with a methoxy (I_{ME}) using Eq. (4) [37].

$$C_{\text{ME}} = 100 \times \frac{5 \times I_{\text{ME}}}{5 \times I_{\text{ME}} + 9 \times I_{\text{TAG}}} \quad (4)$$

RESULTS AND DISCUSSION

Synthesis and Characterization of $\text{SO}_4^{2-}/\text{ZrO}_2$ Solid Acid Catalysts

Catalyst synthesis studies on various H_2SO_4 concentrations were conducted to determine the effect of the concentration of H_2SO_4 on the acidity properties of the catalyst. Characterization using FTIR explains the existence of a functional group owned by a material. Fig. 1 gives information on the differences in the absorption peaks for each catalyst. The absorption of the functional sulfate group belongs to the wavenumber of 750–1350 cm^{-1} . Absorption at that wavenumber is characteristic of inorganic chelate formation where sulfate ions bidentate coordinate with metal cation [38].

The sharpness of the peak for the three catalysts at wavenumbers between 1000–1300 cm^{-1} looks fluctuating. The absorption peak of catalyst at a concentration of 0.5 M H_2SO_4 looks sharper than the others, but the decline in transmittance is followed by a decrease in transmittance

at other wavenumbers. These indications do not show the catalyst acidity with a concentration of H_2SO_4 0.5 M greater than 0.7 M due to decreased transmittance on the spectra. On the other hand, the absorption of ZrO_2 catalyst with a concentration of H_2SO_4 0.7 M appears blunter than other catalysts. It can be analyzed that the vibrations which tend to be detected are sulfate groups dispersed on ZrO_2 . Pavia et al. [39] explained that the vibration of the S–O bond of the sulfonate group was in the absorption band 1000–750 cm^{-1} , which was marked by the appearance of several peaks, whereas the S=O bond had asymmetric and symmetry stretch vibrations detected at 1350 and 1175 cm^{-1} , respectively.

The results of the acidity test on various H_2SO_4 concentrations are listed in Table 1 to strengthen the analysis. The total acidity is obtained from the number of ammonia bases absorbed in the catalyst. Total acidity is defined as the total number of sites of Brønsted and Lewis acids in mmol g^{-1} . Catalysts synthesized using

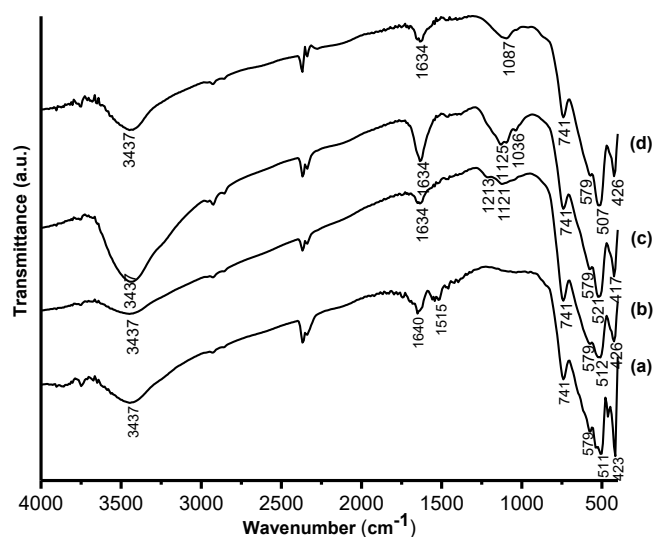


Fig 1. FTIR spectra of (a) ZrO_2 and $\text{SO}_4^{2-}/\text{ZrO}_2$ 60 °C; 24 h catalyst on various H_2SO_4 concentration (b) 0.3 M, (c) 0.5 M, and (d) 0.7 M

Table 1. The result of the acidity test of $\text{SO}_4^{2-}/\text{ZrO}_2$ catalyst on various H_2SO_4 concentrations

Catalyst	Total acidity (mmol g^{-1})
0.3 M $\text{SO}_4^{2-}/\text{ZrO}_2$ 60 °C; 24 h	0.68
0.5 M $\text{SO}_4^{2-}/\text{ZrO}_2$ 60 °C; 24 h	1.35
0.7 M $\text{SO}_4^{2-}/\text{ZrO}_2$ 60 °C; 24 h	1.86

H_2SO_4 0.7 M has a total acidity of 1.86 mmol g^{-1} . That acidity value is higher than ZrO_2 , with a total acidity of 0.06 mmol g^{-1} . The results show that a greater concentration of sulfuric acid increases the total acidity. Increased total acidity correlated with the formation of the number of acid sites. The addition of H_2SO_4 will initiate the formation of sulfate ion coordination to the Zr site. The coordination of sulfate groups on ZrO_2 adds acidic sites to the surface. The super acidic properties of this material can be related to the formation of S=O, which is naturally formed in the complex due to the interaction between ZrO_2 and sulfate ions so that the S=O group provides a strong induction effect [21].

The study of the effect of calcination temperature aims to determine the ZrO_2 crystal phase transformation. The results of FTIR characterization of 0.7 M $\text{SO}_4^{2-}/\text{ZrO}_2$ 60 °C; 24 h catalyst on various calcination temperatures are shown in Fig. 2. The absorption bands at the wavenumbers of 429, 518, 585, 740, 1633, and 3426 cm^{-1} are detected on each catalyst. The FTIR spectra of the catalyst after sulfonation can be observed with the appearance of an absorption band at the wavenumber 1045 cm^{-1} , which is the vibration of the O=S=O group [40]. The vibration of the $-\text{SO}_3\text{H}$ group is detected at 1149 cm^{-1} . The absorption band at 1237 cm^{-1} is the vibration of S–O [41]. The appearance of absorption at 3426 cm^{-1} is suspected of the vibration from the $-\text{SO}_2\text{OH}$ group [42]. The absorption bands at 990, 1050–1060, 1130–1140, and 1220–1230 cm^{-1} indicate the coordination of sulfate bidental ion in Zr^{4+} . The FTIR spectra do not show that the existence of that group significantly changes after being calcined.

The results of the acidity test of the catalysts in various calcination temperatures are displayed in Table 2. The total acidity of the catalyst decreases as the calcination temperature increases. These changes indicate a strong interaction between sulfate anion with ZrO_2 [43]. Sulfur is estimated to reach the highest oxidation level of S^{6+} as SO_4^{2-} as the main species when heated. The increase in heat energy will break the bond between sulfate and ZrO_2 , so catalyst acidity decreases.

The catalyst phase structure influences the selectivity of chemical reactions. Zirconium dioxide in the

tetragonal phase is more sensitive than ZrO_2 in the monoclinic phase. In addition, the specific surface area and appropriate pore size also affect the performance of catalysts in reaction. Sulfate anions that enter the zirconia framework can increase the thermal stability of the material. Incorporating a functional acid group can improve the catalytic acid site to be used as a catalyst in biodiesel production [16].

Adsorption of oxygen ions on the surface of ZrO_2 can trigger phase transformation [23]. Shi et al. [38] explained that the monoclinic crystal phase is very influential in impregnating sulfate groups on the zirconia surfaces. This influence is related to the inhibition of Zr^{3+} formation in the monoclinic phase. The formation of Zr^{3+} can occur in the presence of an oxygen vacancy in the tetragonal phase. Thus, more sulfate groups can bind to the surface of the zirconia. The more sulfate groups that can be impregnated, the acidity site will increase along with the increased catalysis activity [38].

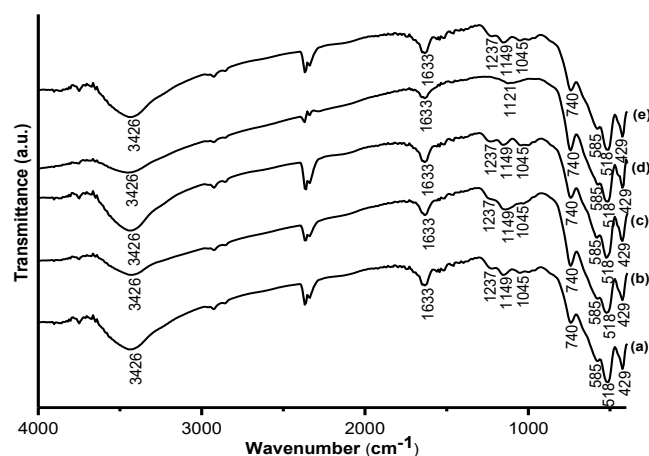


Fig 2. FTIR spectra of 0.7 M $\text{SO}_4^{2-}/\text{ZrO}_2$ 60 °C; 24 h catalyst on various calcination temperature (a) 400, (b) 500, (c) 600, (d) 700, and (e) 800 °C

Table 2. The result of the acidity test of 0.7 M $\text{SO}_4^{2-}/\text{ZrO}_2$ 60 °C; 24 h catalyst on the various calcination temperature

Catalyst	Total acidity (mmol g^{-1})
0.7 M $\text{SO}_4^{2-}/\text{ZrO}_2$ -400	0.67
0.7 M $\text{SO}_4^{2-}/\text{ZrO}_2$ -500	0.46
0.7 M $\text{SO}_4^{2-}/\text{ZrO}_2$ -600	0.24
0.7 M $\text{SO}_4^{2-}/\text{ZrO}_2$ -700	0.12
0.7 M $\text{SO}_4^{2-}/\text{ZrO}_2$ -800	0.11

The result of the catalyst characterization using the XRD is shown in Fig. 3. Based on PDF 01-089-9066, the entire peaks appear on the XRD patterns showing a monoclinic ZrO_2 . Increasing temperature up to 800 °C does not change the catalyst phase $0.7 \text{ M SO}_4^{2-}/\text{ZrO}_2$. No significant changes can be observed at $2\theta = 28.21^\circ$ and 31.46° [44].

Morphology of ZrO_2 and $0.7 \text{ M SO}_4^{2-}/\text{ZrO}_2$ 60 °C; 24 h catalyst are shown in Fig. 4. ZrO_2 has an irregular shape. The size of the material becomes smaller and uniform, with an imperfect round shape after sulfation. Spherical particles tend to have good reactant transport properties. The use of strong acids triggers framework shrinkage and damage some bonds, resulting in smaller particle sizes and changes in passageways between materials. Based on the results of the EDS compiled in Table 3, the sulfur on the surface of ZrO_2 reached 1.07%. The dot mapping results show that the sulfur element is evenly distributed and does not show clumping on any particular side.

The performance of this catalyst is determined by the strength and accessibility of the active acid site to large compounds such as triglycerides and FFA [45]. The physical properties of the catalyst obtained using N_2

adsorption and pore size analysis of the catalyst are summarized in Table 3. Based on these results, it can be seen that the incorporation of sulfuric acid groups in

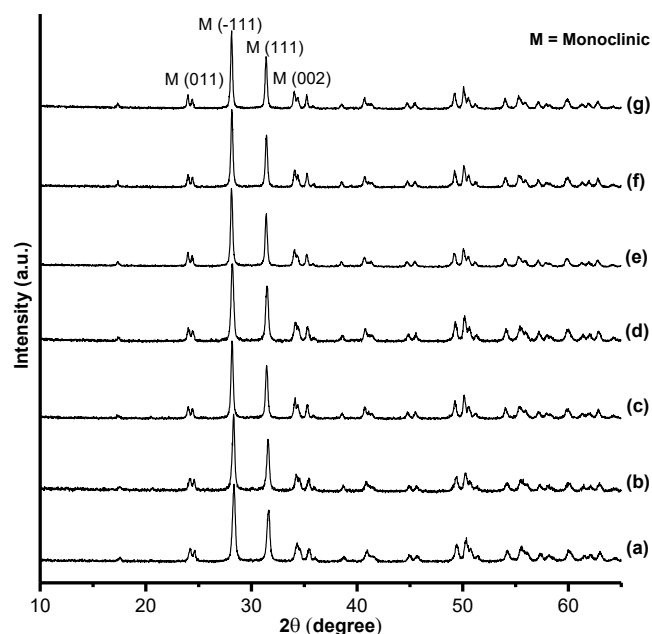


Fig 3. The XRD patterns of catalyst (a) ZrO_2 , (b) $0.7 \text{ M SO}_4^{2-}/\text{ZrO}_2$ 60 °C; 24 h at the calcination temperature (c) 400, (d) 500, (e) 600, (f) 700, and (g) 800 °C

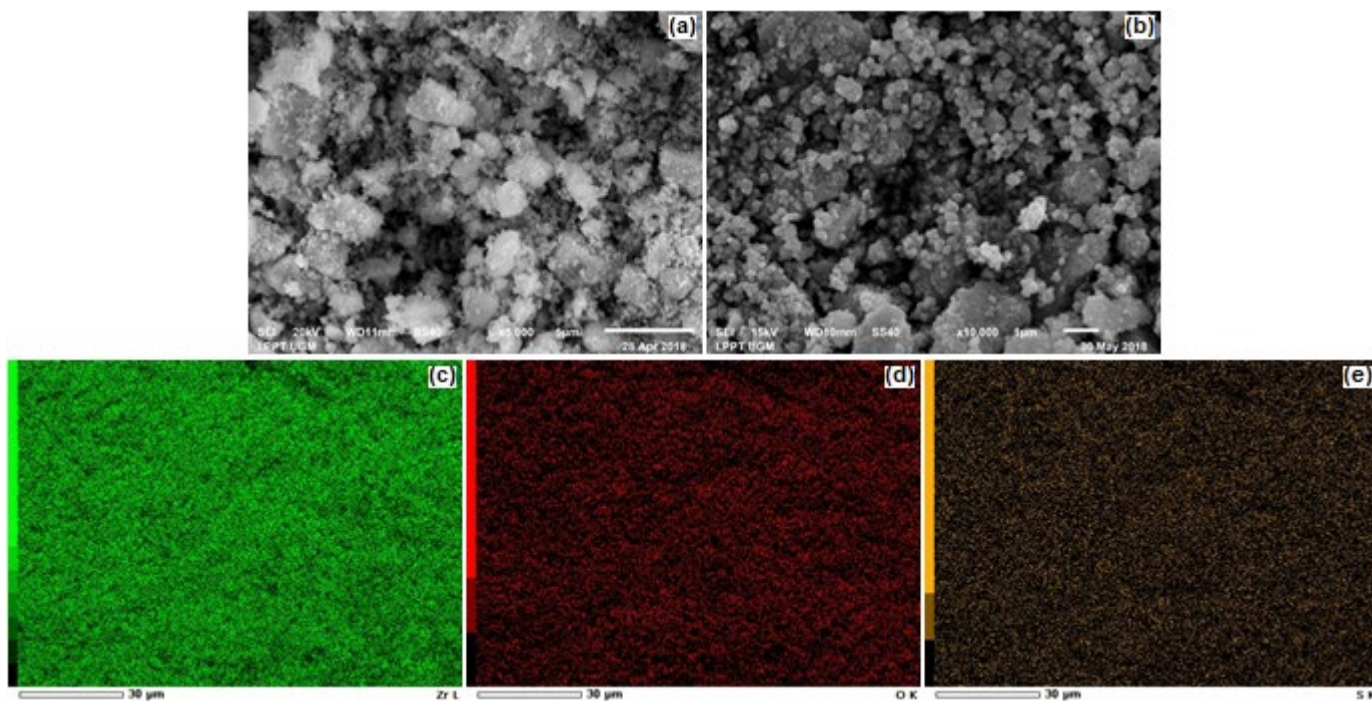


Fig 4. SEM images of catalyst (a) ZrO_2 at magnification 5000 \times , (b) $0.7 \text{ M SO}_4^{2-}/\text{ZrO}_2$ 60 °C; 24 h at magnification 10.000 \times , the dot mapping element of (c) zirconium (d) oxygen and (e) sulfur

Table 3. The elemental composition and surface area analysis of the acid catalyst

Catalyst	% of Element mass			Properties		
	Zr	O	S	S _{BET} ^a (m ² g ⁻¹)	V _p ^b (cm ³ g ⁻¹)	D _p ^c (Å)
ZrO ₂	69.67	25.20	-	13.95	1.74 × 10 ⁻²	25.02
0.7 M SO ₄ ²⁻ /ZrO ₂ 60 °C; 24 h	64.52	28.48	1.07	9.21	1.25 × 10 ⁻²	27.19

^a Specific surface area^b Pore diameter^c Pore volume taken at P/P₀ = 0.90

zirconia decreases the pore volume and surface area of the sulfated zirconia catalyst. The surface area of the catalyst decreased to 9.21 m² g⁻¹. The sulfur element has a diameter of 1.02 Å. An increase in pore diameter is possible due to damage to the structure by acids and the formation of bonds between S and ZrO₂. The interaction between sulfate ions and ZrO₂ protects the catalyst from sintering [21].

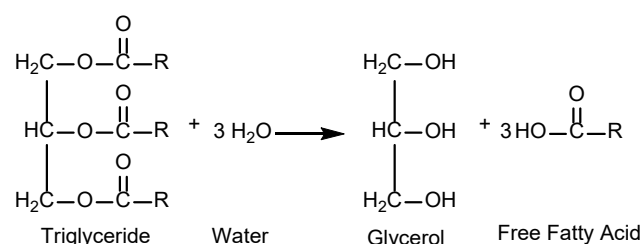
The pore size of the synthesized catalyst is around 27.19 Å. Triglyceride molecules have a dimension of 2.5 nm and can easily fit into the internal surface of the catalyst so that the reaction can take place on the entire catalyst's active site. Large reactants such as triglycerides are not restricted to access catalytic sites. Catalytic activity occurs on external and internal surfaces [31].

Application of SO₄²⁻/ZrO₂ Solid Acid Catalyst on Esterification Reactions

Esterification is part of an organic reaction that aims to form an ester of a mixture of acid and alcohol. In this research, biodiesel was made from the raw material of LGCPO. LGCPO was produced from the palm oil industry, so it needs to be filtered and evaporated. A heterogeneous catalyst is easily degraded by H₂O [3]. The presence of water acts as an impurity. Water will block the active site of the catalyst, which causes its catalytic activity to diminish. Triglycerides will be hydrolyzed to form glycerol and FFA. FFA in LGCPO will react with a basic catalyst to form soap which deactivates the catalyst and makes the separation process more difficult. The scheme of triglycerides hydrolysis is illustrated in Fig. 5.

Effect of wt.% catalyst on %FFA LGCPO

The concentration of FFA is denoted in %FFA. The FFA concentration in the LGCPO is 1.40%. %FFA of each reaction at various conditions is presented in Table 4. There

**Fig 5.** Schematic of triglycerides hydrolysis

is a tendency that shows an increase in wt.% of the catalyst inversely with %FFA. The more amount of catalysts used, the lower the acidity of the oil. The lowest %FFA is obtained when the wt.% of catalyst used is 7%. The esterification reaction that took place using 7 wt.% of catalyst can reduce acidity by 58.01%. Decreasing oil acidity can be attributed to the conversion of FFA to ester. The greater the number of catalysts, the more catalytic's active sites are available for the reaction.

Effect of the molar ratio of LGCPO to methanol on %FFA LGCPO

The molar ratio of LGCPO to methanol is a factor that influences the reduction of FFA concentration. The addition of excess alcohol can accelerate the reaction and is preferred in the formation of biodiesel. Theoretically, the formation of one mole Fatty Acid Methyl Esters (FAME) and one mole of water requires one mole of methanol and one mole of FFA. Excess methanol is needed so the reaction equilibrium shifts towards the product, updating the catalyst surface by removing water molecules from surfaces and regenerating catalytic sites [10,31].

The reduction of %FFA is directly proportional to the molar ratio of methanol. A significant reduction in %FFA is observed at a molar ratio of 1:6. At larger ratios, the FFA decreases until it reaches a maximum reduction

Table 4. The results of %FFA LGCPO in the esterification reaction on various parameters

Catalyst type	Reaction parameters			FFA concentration (%)
	wt.% Catalyst (%)	Molar ratio LGCPO:methanol	Reaction time (min)	
Without catalyst	-	1:12	20	1.24
ZrO ₂	7	1:12	20	1.08
0.7 M SO ₄ ²⁻ /ZrO ₂ 60 °C; 24 h	1	1:9	20	1.10
0.7 M SO ₄ ²⁻ /ZrO ₂ 60 °C; 24 h	3	1:9	20	0.85
0.7 M SO ₄ ²⁻ /ZrO ₂ 60 °C; 24 h	5	1:9	20	0.81
0.7 M SO ₄ ²⁻ /ZrO ₂ 60 °C; 24 h	7	1:3	20	1.24
0.7 M SO ₄ ²⁻ /ZrO ₂ 60 °C; 24 h	7	1:6	20	0.68
0.7 M SO ₄ ²⁻ /ZrO ₂ 60 °C; 24 h	7	1:9	20	0.59
0.7 M SO ₄ ²⁻ /ZrO ₂ 60 °C; 24 h	7	1:12	20	0.44
0.7 M SO ₄ ²⁻ /ZrO ₂ 60 °C; 24 h	7	1:12	40	0.58
0.7 M SO ₄ ²⁻ /ZrO ₂ 60 °C; 24 h	7	1:12	60	0.58
0.7 M SO ₄ ²⁻ /ZrO ₂ 60 °C; 24 h-500	7	1:12	20	1.01

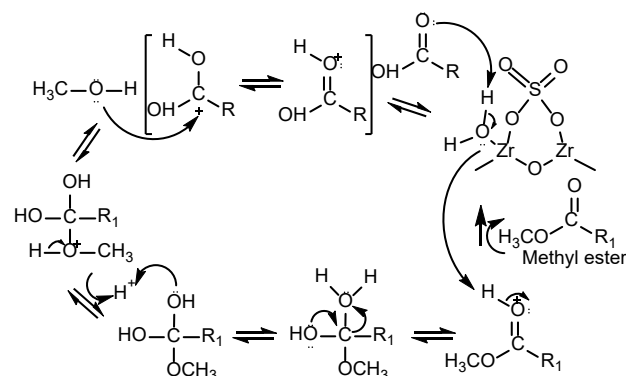
of 68.87% when the molar ratio was 1:12. The more methanol used, the more the formation of methoxy species will be, the reaction will eventually shift towards the product. At low ratios, the produced methoxy ions are also low, so the yield is slight. If the molar ratio is too low, the oil volume fraction in the mixture is high. Then it greatly allows the catalyst to be at the oil phase. The oil covers the catalyst surface then reduces the formation of methoxy ions so that the yield decreases. The oil and methanol interface areas depend on the dispersion of these solutions with each other [46]. Improved interface area makes it easier to transfer methoxy ions faster from the aqueous phase to the organic phase.

Effect of reaction time on %FFA LGCPO

The influence of time reaction was carried out for 20, 40, and 60 min. The addition of reaction time does not give a significant reduction. The best reduction of %FFA lasts for 20 min, giving a decline of 68.87%. Mass transfer between oil and alcohol will increase when the given residence time is longer [10]. The optimum time needed in this reaction is 20 min. The mixture is sufficiently dispersed during this time. Increasing the reaction time will shift the equilibrium towards the reactants because the reaction is reversible and triggers the deactivation of the -SO₃H acid site due to bonds with a polar molecule from reaction mixtures such as H₂O [42]. The prediction

of the mechanism of esterification reaction on SO₄²⁻/ZrO₂ solid acid catalyst are shown in Fig. 6 and 7.

The esterification reaction is carried out under different conditions to examine the performance of the catalyst [47]. The reaction within 20 min without a catalyst resulted in an 11.24% reduction. Sulfated zirconia can reduce FFA up to 68.87%. This value shows that SO₄²⁻/ZrO₂ catalyst has better performance than ZrO₂. Therefore, it can be confirmed that modification using H₂SO₄ improves catalyst performance. The %FFA test results show that the performance of the SO₄²⁻/ZrO₂ catalyst calcined at 500 °C decreased. This data supports that the acidity of the catalyst greatly influences the catalyst performance.

**Fig 6.** Prediction of the esterification reaction mechanism on Brønsted acid site of SO₄²⁻/ZrO₂ solid acid catalyst

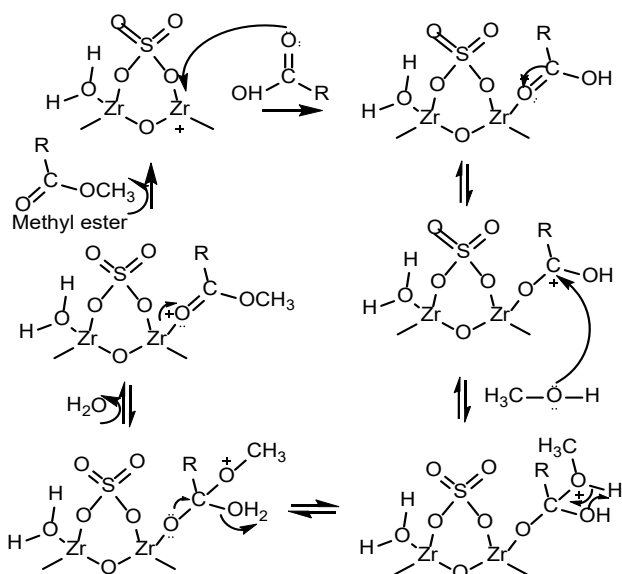


Fig 7. Prediction of the esterification reaction mechanism on Lewis acid site of $\text{SO}_4^{2-}/\text{ZrO}_2$ solid acid catalyst

Synthesis and Characterization of $\text{Na}_2\text{O}/\text{ZrO}_2$ Solid Base Catalysts

Characterization of the catalyst using FTIR on various NaOH concentrations is shown in Fig. 8. This study is carried out to determine the effect of the amount of NaOH on the basic properties of the base catalyst. The FTIR spectra show that each catalyst has absorption at wavenumbers 422, 500, 583, 745, 871, 1455, 1637, and 3432 cm^{-1} . The $\text{Na}_2\text{O}/\text{ZrO}_2$ catalyst can absorb CO_2 from the environment. The greater concentration of base that is given in the reaction, the more CO_2 will be absorbed. As a result, the CO_3^{2-} absorption band appears even sharper. There are several changes observed in Fig. 8. The sharpness of the vibration of Zr-O-Na asymmetry detected at 1637 cm^{-1} decreases with the increasing concentration of NaOH. This is possibly due to the large addition of Na covering the substrate surface. Based on Table 5, the catalyst that uses NaOH 4 M has the highest total basicity value. The addition of sodium ions triggers the formation of strong basic sites. Active sites increase with the increasing number of alkali metals on ZrO_2 [28].

The FTIR spectra of 4 M $\text{Na}_2\text{O}/\text{ZrO}_2$ $60\text{ }^\circ\text{C}$; 12 h catalyst on various calcination temperatures are shown in Fig. 9. Absorption bands at wavenumbers 423, 500, 576, 750, 865, 1446, 1577, 2852, 2918, and 3420 cm^{-1} are

detected on each catalysts. In general, there is a tendency that shows a decrease in the sharpness of vibration CO_3^{2-} . These results are confirmed by the basicity test results given in Table 6, which show that the basicity of the

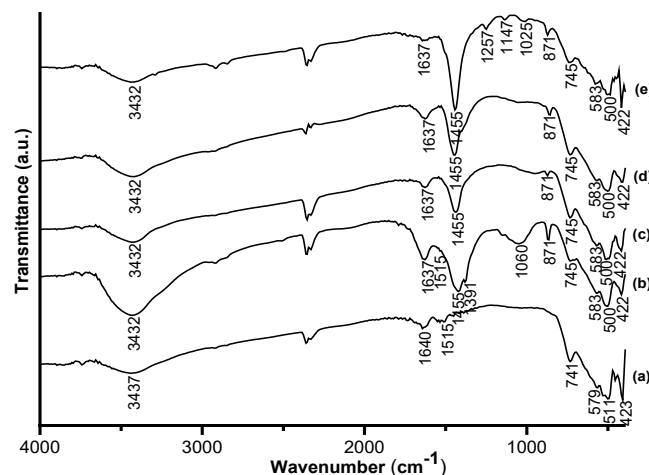


Fig 8. FTIR spectra of (a) ZrO_2 and $\text{Na}_2\text{O}/\text{ZrO}_2$ $60\text{ }^\circ\text{C}$; 12 h catalyst on various NaOH concentration (b) 1 M, (c) 2 M, (d) 3 M, and (e) 4 M

Table 5. The result of basicity test of $\text{Na}_2\text{O}/\text{ZrO}_2$ catalyst on various NaOH concentrations

Catalyst	Total basicity (mmol g^{-1})
1 M $\text{Na}_2\text{O}/\text{ZrO}_2$ $60\text{ }^\circ\text{C}$; 12 h	0.56 ± 0.01
2 M $\text{Na}_2\text{O}/\text{ZrO}_2$ $60\text{ }^\circ\text{C}$; 12 h	1.43 ± 0.04
3 M $\text{Na}_2\text{O}/\text{ZrO}_2$ $60\text{ }^\circ\text{C}$; 12 h	1.83 ± 0.02
4 M $\text{Na}_2\text{O}/\text{ZrO}_2$ $60\text{ }^\circ\text{C}$; 12 h	3.75 ± 0.12

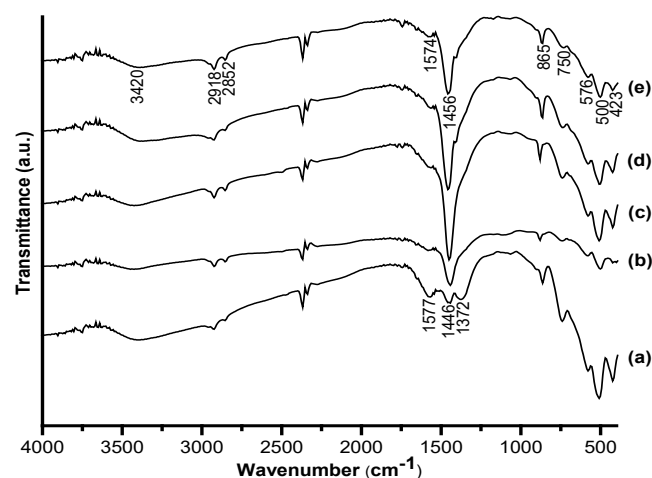


Fig 9. FTIR spectra of 4 M $\text{Na}_2\text{O}/\text{ZrO}_2$ $60\text{ }^\circ\text{C}$; 12 h catalyst on various calcination temperature (a) 400, (b) 500, (c) 600, (d) 700, and (e) $800\text{ }^\circ\text{C}$

catalyst tends to decrease after calcination. The result of catalyst characterization using XRD is shown in Fig. 10. The existence of the monoclinic ZrO_2 phase is characterized by the appearance of peaks at $2\theta = 28.21^\circ$ and 31.46° . Temperature rising to $800^\circ C$ does not change the catalyst phase.

Fig. 11 shows the SEM image of 4 M Na_2O/ZrO_2 $60^\circ C$; 12 h at a magnification of 1000 \times and 3000 \times . The size of the material becomes smaller and uniform with the forms of granules that overlap each other. Based on the results of EDS compiled in Table 7, Na dispersed on the surface of ZrO_2 reached 8.41%. The results of the physical properties characterization of catalysts are reported in Table 7. Based on these results, it can be seen that modified zirconia has decreased pore volume and surface area. The surface area of the modified catalyst has decreased to $10.38\text{ m}^2\text{ g}^{-1}$. These changes are related to changes in the surface of the catalyst. Na covers the surface of the pore of the catalyst [48]. The detected pores are pseudo pores.

Application of Na_2O/ZrO_2 Solid Base Catalyst for Transesterification Reaction

At this stage, the esterified LGCPO with the lowest FFA concentration is used as a source of triglycerides. The reaction temperature is chosen at the optimum temperature of $55^\circ C$. The optimum temperature is the temperature that closes to the boiling point of methanol, where methanol is

Table 6. The result of basicity test of 4 M Na_2O/ZrO_2 $60^\circ C$; 12 h catalyst on the various calcination temperature

Catalyst	Total basicity (mmol g^{-1})
4 M Na_2O/ZrO_2 -400	3.07 ± 1.06
4 M Na_2O/ZrO_2 -500	3.03 ± 0.06
4 M Na_2O/ZrO_2 -600	2.98 ± 0.05
4 M Na_2O/ZrO_2 -700	2.68 ± 0.49
4 M Na_2O/ZrO_2 -800	2.58 ± 0.07

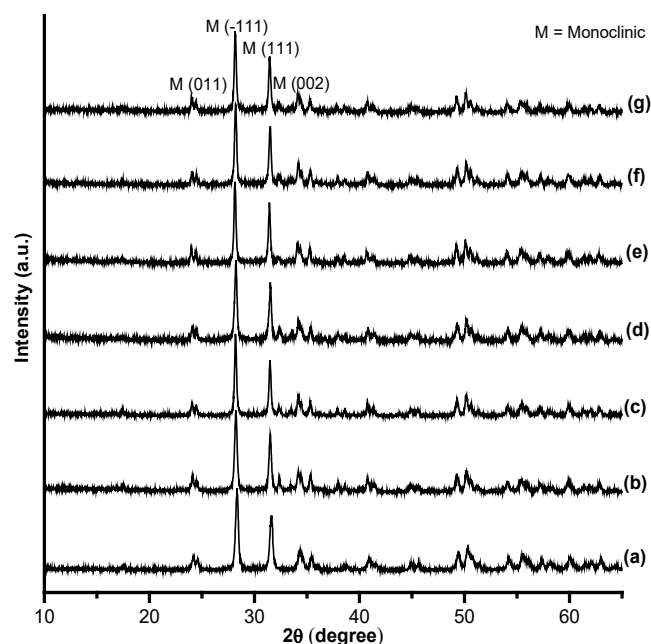


Fig 10. The XRD patterns of catalyst (a) ZrO_2 , (b) 4 M Na_2O/ZrO_2 $60^\circ C$; 12 h at the calcination temperature (c) 400, (d) 500, (e) 600, (f) 700, and (g) $800^\circ C$

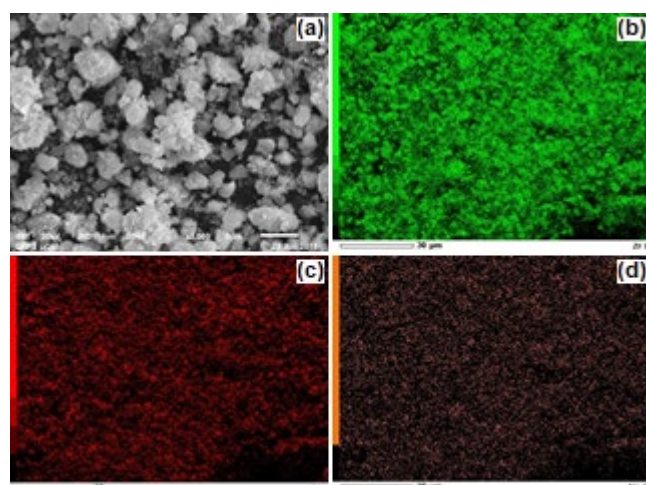


Fig 11. (a) SEM image of 4 M Na_2O/ZrO_2 $60^\circ C$; 12 h catalyst at magnification 3000 \times , the dot mapping element of (b) zirconium (c) oxygen and (d) sodium

Table 7. The elemental composition and surface area analysis of the base catalyst

Catalyst	% of Element mass			Properties		
	Zr	O	Na	S_{BET}^a ($m^2\text{ g}^{-1}$)	V_p^b ($cm^3\text{ g}^{-1}$)	D_p^c (\AA)
ZrO_2	69.67	25.20	-	13.95	1.74×10^{-2}	25.02
4 M Na_2O/ZrO_2 $60^\circ C$; 12 h	42.65	38.28	8.41	10.38	1.35×10^{-2}	25.97

^a Specific surface area

^b Pore diameter

^c Pore volume taken at $P/P_0 = 0.90$

in the liquid phase. At temperatures above the boiling point, the methanol is evaporated to reduce the contact interface [46]. Fig. 12 presents the results of FTIR characterization of LGCPO and transesterification compound. According to Pavia et al. [39], C–O vibrations in esters are indicated by strong absorption at 1300–1000 cm^{-1} , while C=O is at 1850–1650 cm^{-1} . This shift is affected by the dipole moment. Oxygen on the ester triggers an increase in frequency in that area. The results of the interpretation of functional groups are summarized in Table 8. The biodiesel content is determined using gas chromatography. The chromatogram of the transesterified compound is presented in Fig. 13. The results of the transesterified compound are listed in Table 9.

Transesterification and LGCPO compounds analyzed by a $^1\text{H-NMR}$ spectrometer are shown in Fig. 14 and 15. The results of the analysis are used to confirm the presence of compounds based on the proton environment. An indication that shows the success of transesterification is the appearance of an ester group from triglycerides or FFA.

Based on the results of the LGCPO $^1\text{H-NMR}$ in Fig. 15, there is a peak that appears in the chemical shift $\delta = 4.3$ ppm indicating the presence of triglycerides [49]. The characteristic chemical shift of esters compound shows at 2.1 to 2.5 ppm and 3.5 to 4.8 ppm [39]. The presence of peak with triplet integrated at 0.88 ppm indicates the proton of methyl groups. The peak is in the most upfield area, which shows the proton in the least protected environment and is not affected by the induction of other protons.

The methoxy group shows a peak at 3.66 ppm with a singlet pattern. The peak is in a shifting area that is more

downfield than the other peaks. The shift is influenced by the pull of electron clouds of carbonyl groups and induction of methoxy groups ($-\text{OCH}_3$ $\delta = 3.66$ ppm is 2.59), while triglycerides in LGCPO have integration of 0.66. Methyl ester conversion is calculated from the integration of triglycerides and methyl esters [37]. The

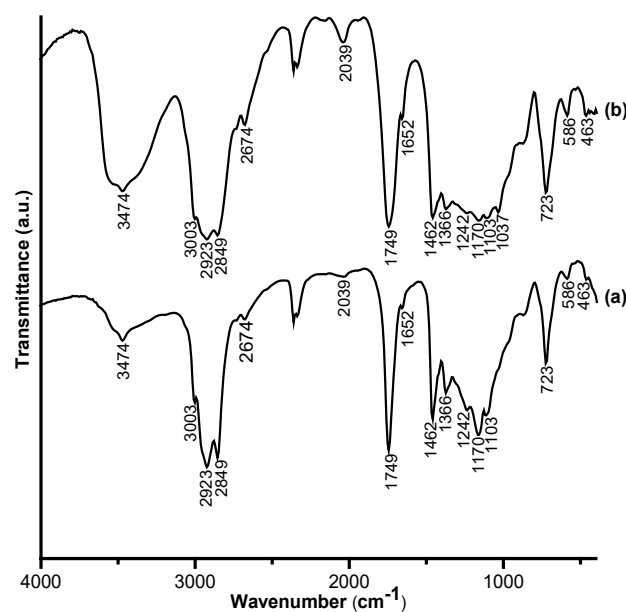


Fig 12. FTIR spectra of (a) LGCPO dan (b) transesterified compound

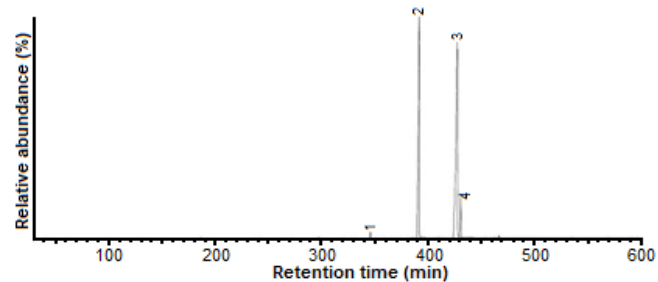


Fig 13. Chromatogram of transesterified compounds

Table 8. Interpretation of FTIR spectra of LGCPO and transesterified compound

Functional group	Vibration type	Wavenumber (cm^{-1})	
		LGCPO	Transesterified compound
–OH	Stretching	3474	3474
–CH ₂	Asymmetry stretching	2923	2923
–CH ₂	Symmetry stretching	2849	2849
–C=O	Stretching	1749	1749
–CH ₂	Shear-type	1462	1462
–CH ₃	Bending	1366	1366
C–O–C	Symmetry stretching	1170	1170
–CH ₂	Plane rocking	723	723

Table 9. The interpretation of the chromatogram of transesterified compound

Peak	Retention time (min)	Compound	Molecular formula	Molecular weight (g mol ⁻¹)	Selectivity (%)
1	34.6	Methyl Miristate	C ₁₅ H ₃₀ O ₂	242	0.56
2	39.2	Methyl Palmitate	C ₁₇ H ₃₄ O ₂	270	43.36
3	42.7	Methyl Oleate	C ₁₉ H ₃₆ O ₂	296	51.51
4	43.1	Methyl Stearate	C ₁₉ H ₃₈ O ₂	298	4.57

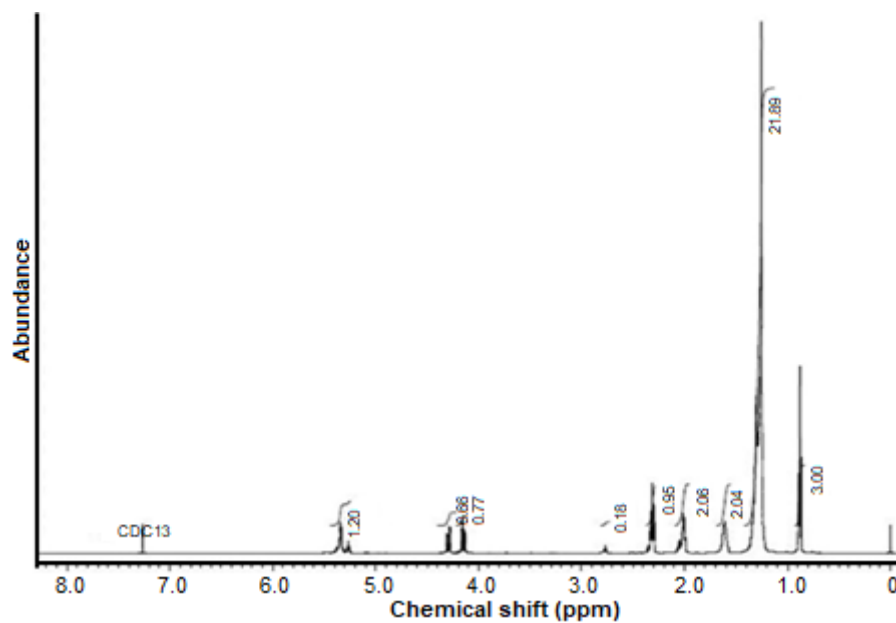
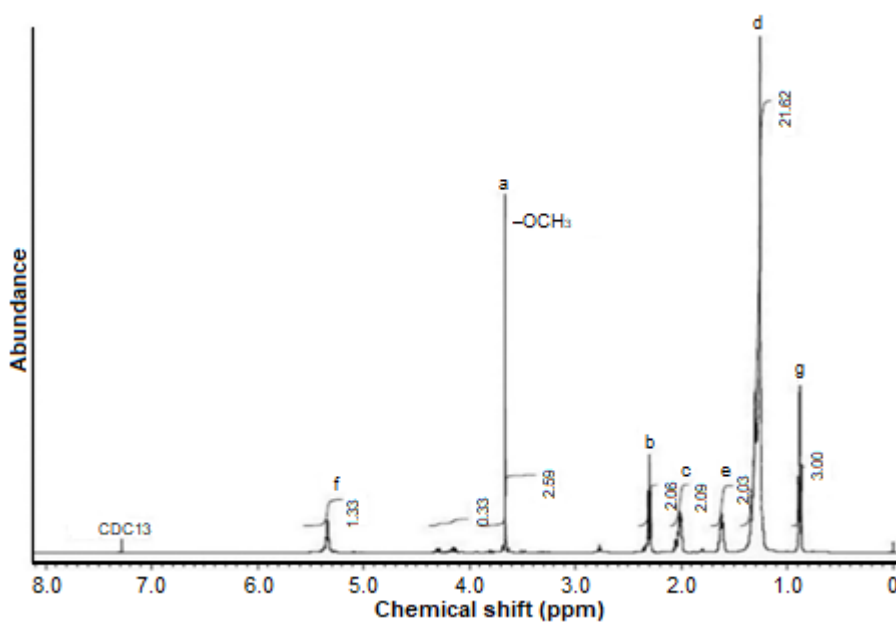
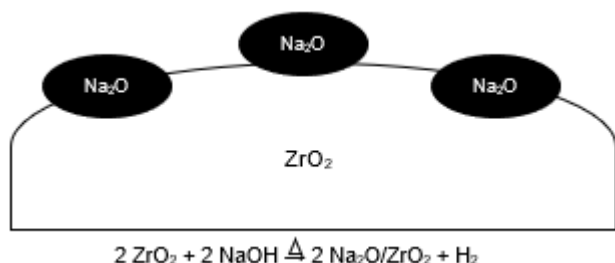
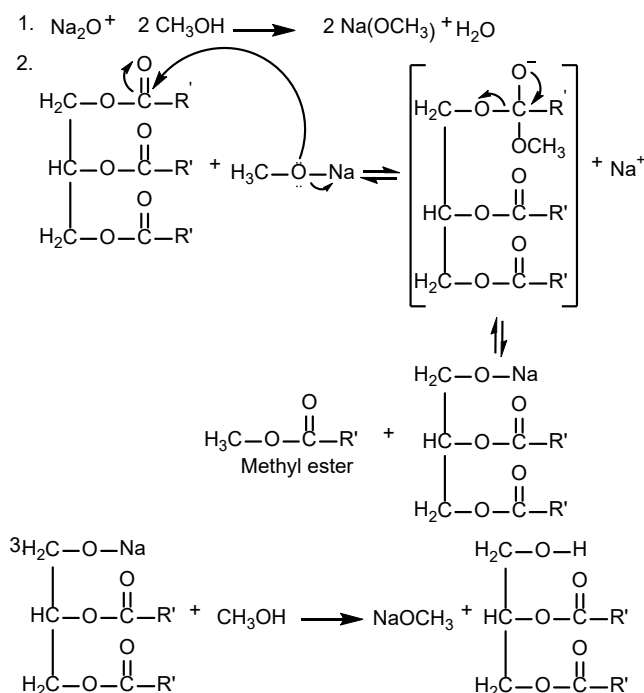
**Fig 14.** ¹H-NMR spectra of LGCPO**Fig 15.** ¹H-NMR spectra of transesterified compound

Table 10. Calculation of methyl esters conversion

Integration of triglycerides (I_{TAG})	Integration of methyl esters (I_{ME})	% of Methyl ester conversion (C_{ME})
0.66	2.59	68.55%

**Fig 16.** The design of $\text{Na}_2\text{O}/\text{ZrO}_2$ solid base catalyst formation as a composite material**Fig 17.** The prediction of the mechanism of transesterification reaction on $\text{Na}_2\text{O}/\text{ZrO}_2$ solid base catalyst

conversion of methyl ester was 68.55%. After being calculated using the Knotee equation referring to Table 10, the conversion of methyl ester is 68.55%.

Base catalysts that were synthesized have characteristics as composite materials. The composition design of the composite material of $\text{Na}_2\text{O}/\text{ZrO}_2$ is illustrated in Fig. 16. Zirconia dioxide has a function as

supporting material. The prediction of the mechanism of transesterification reaction on $\text{Na}_2\text{O}/\text{ZrO}_2$ solid base catalyst is shown in Fig. 17. Na_2O tends to be in the aqueous phase (methanol) because it is hydrophilic. Na_2O polarized CH_3OH to form methoxide ions ($^-\text{OCH}_3$) [50]. Sodium methoxide (NaOCH_3) is on the surface of Na_2O . NaOCH_3 transfers the methoxy group to carbonyl triglycerides to form insoluble organic salts. The alkoxy triglyceride group binds to sodium to form sodium alkoxy and methyl ester. Alkoxy sodium with excess methanol produces sodium methoxide and glycerol (after all stages have been reached).

CONCLUSION

This work demonstrates the synthesis of a solid acid-base catalyst based on ZrO_2 for biodiesel conversion. In summary, the design concept of this catalyst synthesis is to maintain a mixture of ZrO_2 with NaOH or H_2SO_4 under a certain temperature and pressure. The focus is to understand the influence of several parameters in this reaction system on the catalyst's acidity/basicity properties. The evidence has demonstrated the successful preparation of catalysts. The solid acid catalyst of $\text{SO}_4^{2-}/\text{ZrO}_2$ 60 °C; 24 h had the highest total acidity of 1.86 mmol g^{-1} using 0.7 M H_2SO_4 . The solid base catalyst of $\text{Na}_2\text{O}/\text{ZrO}_2$ 60 °C; 12 h has the highest total basicity of 3.75 ± 0.12 mmol g^{-1} using 4 M NaOH . The acidity and basicity of the catalyst increase with the increasing concentration of H_2SO_4 or NaOH . The total acidity of the 0.7 M $\text{SO}_4^{2-}/\text{ZrO}_2$ 60 °C; 24 h solid acid catalyst and the basicity of 4 M $\text{Na}_2\text{O}/\text{ZrO}_2$ 60 °C; 24 h solid base catalyst decreases with increasing calcination temperature. The release of functional groups on the catalyst causes the acidity and basicity of the catalyst to decrease.

Since we are interested in investigating the performance of these catalysts, some important parameters for biodiesel conversion are conducted. The

concentration of FFA decreased to 68.87% after being processed using an optimized acid catalyst. The solid base catalyst of 4 M Na₂O/ZrO₂ 60 °C; 24 h successfully converted LGCPO into biodiesel by 68.55% through a transesterification reaction. The spectroscopic analysis helped to investigate the product. ¹H-NMR revealed the presence of triglycerides ($\delta = 4.3$ ppm) and methoxy groups ($\delta = 3.66$ ppm). The conversion of methyl ester that was obtained is 68.55%. Methyl oleate is the major product, accompanied by other methyl ester compounds, including methyl palmitate, methyl stearate, and a small amount of methyl myristate.

■ ACKNOWLEDGMENTS

The authors are grateful for financial support from the Ministry of Research, Technology and Higher Education of Republic Indonesia through STRANAS Research Grant (contract number 001/SP2H/LT/DRPM/IV/2017) and World Class Research (WCR) 2019 (contract number 1980/UN1.DITLIT/DIT-LIT/LT/2019).

■ REFERENCES

- [1] Hajjari, M., Tabatabaei, M., Aghbashlo, M., and Ghanavati, H., 2017, A review on the prospects of sustainable biodiesel production: A global scenario with an emphasis on waste-oil biodiesel utilization, *Renewable Sustainable Energy Rev.*, 72, 445–464.
- [2] Muanruksa, P., and Kaewkannetra, P., 2020, Combination of fatty acids extraction and enzymatic esterification for biodiesel production using sludge palm oil as a low-cost substrate, *Renewable Energy*, 146, 901–906.
- [3] Atadashi, I.M., Aroua, M.K., Aziz, A.R.A., and Sulaiman, N.M.N., 2013, The effects of catalysts in biodiesel production: A review, *J. Ind. Eng. Chem.*, 19 (1), 14–26.
- [4] Li, Y., Ye, B., Shen, J., Tian, Z., Wang, L., Zhu, L., Ma, T., Yang, D., and Qiu, F., 2013, Optimization of biodiesel production process from soybean oil using the sodium potassium tartrate doped zirconia catalyst under Microwave Chemical Reactor, *Bioresour. Technol.*, 137, 220–225.
- [5] Hasanudin, H., Rachmat, A., Said, M., and Wijaya, K., 2020, Kinetic model of crude palm oil hydrocracking over Ni/Mo ZrO₂-pillared bentonite catalyst, *Period. Polytech., Chem. Eng.*, 64 (2), 238–247.
- [6] Hayyan, A., Mjalli, F.S., Hashim, M.A., Hayyan, M., AlNashef, I.M., Al-Wahaibi, T., and Al-Wahaibi, Y.M., 2014, A solid organic acid catalyst for the pretreatment of low-grade crude palm oil and biodiesel production, *Int. J. Green Energy*, 11 (2), 129–140.
- [7] Min Oo, Y., Prateepchaikul, G., and Somnuk, K., 2021, Continuous acid-catalyzed esterification using a 3D printed rotor-stator hydrodynamic cavitation reactor reduces free fatty acid content in mixed crude palm oil, *Ultrason. Sonochem.*, 72, 105419.
- [8] Pua, F., Fang, Z., Zakaria, S., Guo, F., and Chia, C., 2011, Direct production of biodiesel from high-acid value *Jatropha* oil with solid acid catalyst derived from lignin, *Biotechnol. Biofuels*, 4 (1), 56.
- [9] Qu, T., Niu, S., Zhang, X., Han, K., and Lu, C., 2021, Preparation of calcium modified Zn-Ce/Al₂O₃ heterogeneous catalyst for biodiesel production through transesterification of palm oil with methanol optimized by response surface methodology, *Fuel*, 284, 118986.
- [10] Chuah, L.F., Bokhari, A., Yusup, S., Klemeš, J.J., Abdullah, B., and Akbar, M.M., 2016, Optimisation and kinetic studies of acid esterification of high free fatty acid rubber seed oil, *Arabian J. Sci. Eng.*, 41 (7), 2515–2526.
- [11] Rattanaphra, D., Harvey, A.P., Thanapimmetha, A., and Srinophakun, P., 2012, Simultaneous transesterification and esterification for biodiesel production with and without a sulfated zirconia catalyst, *Fuel*, 97, 467–475.
- [12] Roper-Vega, J.L., Aldana-Pérez, A., Gómez, R., and Niño-Gómez, M.E., 2010, Sulfated titania [TiO₂/SO₄²⁻]: A very active solid acid catalyst for the esterification of free fatty acids with ethanol, *Appl. Catal., A*, 379 (1-2), 24–29.
- [13] Johnson, M., Ren, J., Lefler, M., Licht, G., Vicini, J., Liu, X., and Licht, S., 2017, Carbon nanotube wools

- made directly from CO₂ by molten electrolysis: Value-driven pathways to carbon dioxide greenhouse gas mitigation, *Mater. Today Energy*, 5, 230–236.
- [14] Chouhan, A.P.S., and Sarma, A.K., 2011, Modern heterogeneous catalysts for biodiesel production: A comprehensive review, *Renewable Sustainable Energy Rev.*, 15 (9), 4378–4399.
- [15] Devyatkov, S.Y., Zinnurova, A.A., Aho, A., Kronlund, D., Peltonen, J., Kuzichkin, N.V., Lisitsyn, N.V., and Murzin, D.Y., 2016, Shaping of sulfated zirconia catalysts by extrusion: understanding the role of binders, *Ind. Eng. Chem. Res.*, 55 (23), 6595–6606.
- [16] Pan, Y., Zhang, J., Xu, Y., Gao, Y., Chen, Z., and Wang, J., 2016, A facile one-pot hydrothermal process to synthesize sulfonated mesoporous ZrO₂, *J. Porous Mater.*, 23 (2), 489–495.
- [17] Utami, M., Trisunaryanti, W., Shida, K., Tsushida, M., Kawakita, H., Ohto, K., Wijaya, K., and Tominaga, M., 2019, Hydrothermal preparation of a platinum-loaded sulfated nanozirconia catalyst for the effective conversion of waste low density polyethylene into gasoline-range hydrocarbons, *RSC Adv.*, 9 (71), 41392–41401.
- [18] Li, Y., He, D., Zhu, Q., Zhang, X., and Xu, B., 2004, Effects of redox properties and acid-base properties on isosynthesis over ZrO₂-based catalysts, *J. Catal.*, 221 (2), 584–593.
- [19] Rabee, A.I.M., Manayil, J.C., Isaacs, M.A., Parlett, C.M.A., Durnell, L.J., Zaki, M.I., Lee, A.F., and Wilson, K., 2018, On the impact of the preparation method on the surface basicity of Mg–Zr mixed oxide catalysts for tributyrin transesterification, *Catalysts*, 8 (6), 228.
- [20] Noh, H.J., Seo, D.S., Kim, H., and Lee, J.K., 2003, Synthesis and crystallization of anisotropic shaped ZrO₂ nanocrystalline powders by hydrothermal process, *Mater. Lett.*, 57 (16-17), 2425–2431.
- [21] Sohn, J.R., Kim, H.W., Park, M.Y., Park, E.H., Kim, J.T., and Park, S.E., 1995, Highly active catalyst of NiO–ZrO₂ modified with H₂SO₄ for ethylene dimerization, *Appl. Catal., A*, 128 (1), 127–141.
- [22] Saravanan, K., Tyagi, B., and Bajaj, H.C., 2012, Esterification of caprylic acid with alcohol over nano-crystalline sulfated zirconia, *J. Sol-Gel Sci. Technol.*, 62 (1), 13–17.
- [23] Srinivasan, R., Sparks, D.E., and Davis, B.H., 1996, State of platinum in zirconia and sulfated zirconia catalysts, *Catal. Lett.*, 40 (3), 167–173.
- [24] Zhang, C., Miranda, R., and Davis, B.H., 1994, Platinum-sulfated-zirconia. Infrared study of adsorbed pyridine, *Catal. Lett.*, 29 (3), 349–359.
- [25] Popova, M., Szegedi, Á., Lazarova, H., Dimitrov, M., Kalvachev, Y., Atanasova, G., Ristić, A., Wilde, N., and Gläser, R., 2017, Influence of the preparation method of sulfated zirconia nanoparticles for levulinic acid esterification, *React. Kinet., Mech. Catal.*, 120 (1), 55–67.
- [26] Sayilkan, F., Asiltürk, M., Burunkaya, E., and Arpaç, E., 2009, Hydrothermal synthesis and characterization of nanocrystalline ZrO₂ and surface modification with 2-acetoacetoxyethyl methacrylate, *J. Sol-Gel Sci. Technol.*, 51 (2), 182–189.
- [27] Devulapelli, V.G., and Weng, H.S., 2009, Esterification of 4-methoxyphenylacetic acid with dimethyl carbonate over mesoporous sulfated zirconia, *Catal. Commun.*, 10 (13), 1711–1717.
- [28] Qiu, F., Li, Y., Yang, D., Li, X., and Sun, P., 2011, Heterogeneous solid base nanocatalyst: Preparation, characterization and application in biodiesel production, *Bioresour. Technol.*, 102 (5), 4150–4156.
- [29] El-Desouki, D.S., Ibrahim, A.H., Abdelazim, S.M., Aboul-Gheit, N.A.K., and Abdel-Hafizar, D.R., 2021, The optimum conditions for methanol conversion to dimethyl ether over modified sulfated zirconia catalysts prepared by different methods, *J. Fuel Chem. Technol.*, 49 (1), 63–71.
- [30] Pratap, S.R., Shamshuddin, S.Z.M., and Shyamprasad, K., 2020, Microwave assisted synthesis of propyl esters over modified versions of zirconia: Kinetic study, *Chem. Data Collect.*, 30, 100579.
- [31] Essamlali, Y., Amadine, O., Larzek, M., Len, C., and Zahouily, M., 2017, Sodium modified hydroxyapatite: Highly efficient and stable solid-

- base catalyst for biodiesel production, *Energy Convers. Manage.*, 149, 355–367.
- [32] Abedin, M.A., Kanitkar, S., Bhattar, S., and Spivey, J.J., 2021, Methane dehydroaromatization using Mo supported on sulfated zirconia catalyst: Effect of promoters, *Catal. Today*, 365, 71–79.
- [33] Marinković, D.M., Stanković, M.V., Veličković, A.V., Avramović, J.M., Miladinović, M.R., Stamenković, O.O., Veljković, V.B., and Jovanović, D.M., 2016, Calcium oxide as a promising heterogeneous catalyst for biodiesel production: Current state and perspectives, *Renewable Sustainable Energy Rev.*, 56, 1387–1408.
- [34] Helmiyati, H., Budiman, Y., Abbas, G.H., Dini, F.W., and Khalil, M., 2021, Highly efficient synthesis of biodiesel catalyzed by a cellulose@hematite-zirconia nanocomposite, *Heliyon*, 7 (3), e06622.
- [35] dos Santos, L.K., Hatanaka, R.R., de Oliveira, J.E., and Flumignan, D.L., 2019, Production of biodiesel from crude palm oil by a sequential hydrolysis/esterification process using subcritical water, *Renewable Energy*, 130, 633–640.
- [36] Chong, Y.Y., Thangalazhy-Gopakumar, S., Gan, S., Lee, L.Y., and Ng, H.K., 2020, Esterification and neutralization of bio-oil from palm empty fruit bunch fibre with calcium oxide, *Bioresour. Technol. Rep.*, 12, 100560.
- [37] Knothe, G., 2000, Monitoring a progressing transesterification reaction by fiber-optic near infrared spectroscopy with correlation to ^1H nuclear magnetic resonance spectroscopy, *J. Am. Oil Chem. Soc.*, 77 (5), 489–493.
- [38] Shi, G., Yu, F., Wang, Y., Pan, D., Wang, H., and Li, R., 2016, A novel one-pot synthesis of tetragonal sulfated zirconia catalyst with high activity for biodiesel production from the transesterification of soybean oil, *Renewable Energy*, 92, 22–29.
- [39] Pavia, D.L., Lampman, G.M., Kriz, G.S., and Vyvyan, J.A., 2009, Introduction to Spectroscopy, 4th Ed., Brooks/Cole, Cengage Learning, Belmont, CA.
- [40] Liu, N., Ma, Z., Wang, S., Shi, L., Hu, X., and Meng, X., 2020, Palladium-doped sulfated zirconia: Deactivation behavior in isomerization of *n*-hexane, *Fuel*, 262, 116566.
- [41] Navio, J.A., Colón, G., Sánchez-Soto, P.J., and Macias, M., 1997, Effects of H_2O_2 and SO_4^{2-} species on the crystalline structure and surface properties of ZrO_2 processed by alkaline precipitation, *Chem. Mater.*, 9 (5), 1256–1261.
- [42] Tuong, T., Tran, V., Kaiprommarat, S., Kongparakul, S., Reubroycharoen, P., Guan, G., Huan, M., and Samart, C., 2016, Green biodiesel production from waste cooking oil using an environmentally benign acid catalyst, *Waste Manage.*, 52, 367–374.
- [43] El-Dafrawy, S.M., Hassan, S.M., and Farag, M., 2020, Kinetics and mechanism of Pechmann condensation reaction over sulphated zirconia-supported zinc oxide, *J. Mater. Res. Technol.*, 9 (1), 13–21.
- [44] Vannucci, J.A., Nichio, N.N., and Pompeo, F., 2021, Solketal synthesis from ketalization of glycerol with acetone: A kinetic study over a sulfated zirconia catalyst, *Catal. Today*, 372, 238–245.
- [45] Pirez, C., Reche, M.T., Lee, A.F., Manayil, J.C., dos-Santos, V.C., and Wilson, K., 2015, Hydrothermal saline promoted grafting of periodic mesoporous organic sulfonic acid silicas for sustainable FAME production, *Catal. Lett.*, 145 (7), 1483–1490.
- [46] Colombo, K., Ender, L., and Barros, A.A.C., 2017, The study of biodiesel production using CaO as a heterogeneous catalytic reaction, *Egypt. J. Pet.*, 26 (2), 341–349.
- [47] Zhang, H., Luo, X., Shi, K., Wu, T., He, F., Yang, H., Zhang, S., and Peng, C., 2019, Nanocarbon-based catalysts for esterification: Effect of carbon dimensionality and synergistic effect of the surface functional groups, *Carbon*, 147, 134–145.
- [48] Chang, A., Pan, J.H., Lai, N.C., Tsai, M.C., Mochizuki, T., Toba, M., Chen, S.Y., and Yang, C.M., 2020, Efficient simultaneous esterification/transesterification of non-edible *Jatropha* oil for biodiesel fuel production by template-free synthesized nanoporous titanosilicates, *Catal. Today*, 356, 56–63.

- [49] Shah, K.A., Parikh, J.K., and Maheria, K.C., 2014, Optimization studies and chemical kinetics of silica sulfuric acid-catalyzed biodiesel synthesis from waste cooking oil, *Bioenergy Res.*, 7 (1), 206–216.
- [50] Saravana Sathiya Prabhakar, R., Benitha, V.S., and Nagarajan, J., 2021, Improved yield of palm oil biodiesel through nano catalytic transesterification, *Mater. Today: Proc.*, 46, 8433–8437.